Table A–15

Charts of Theoretical Stress-Concentration Factors K_t^*

Figure A–15–1

Bar in tension or simple compression with a transverse hole. $\sigma_0 = F/A$, where $A = (w - d)t$ and t is the thickness.

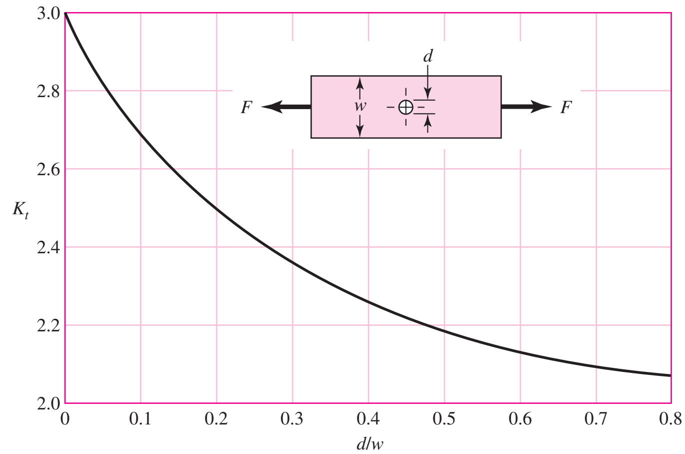

Figure A–15–2

Rectangular bar with a transverse hole in bending. $\sigma_0 = Mc/I$, where $I = (w - d)h^3/12$.

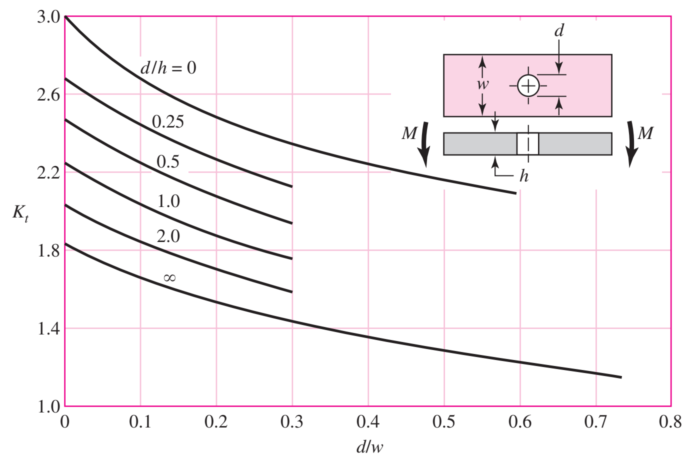

Figure A–15–3

Notched rectangular bar in tension or simple compression. $\sigma_0 = F/A$, where $A = dt$ and t is the thickness.

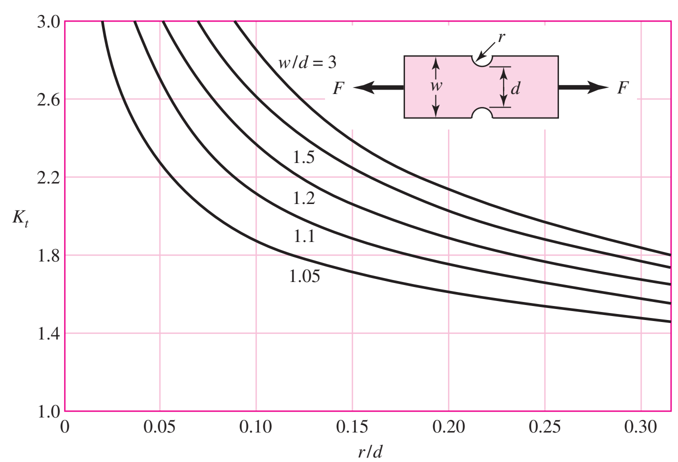

Table A–15

Charts of Theoretical Stress-Concentration Factors K_t^* *(Continued)*

Figure A–15–4

Notched rectangular bar in bending. $\sigma_0 = Mc/I$, where $c = d/2$, $I = td^3/12$, and t is the thickness.

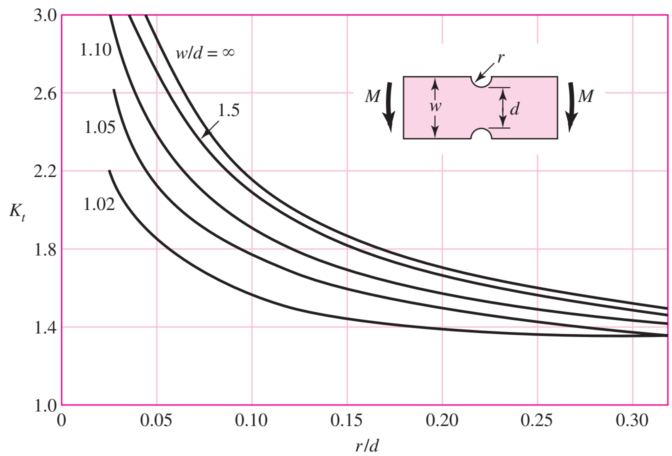

Figure A–15–5

Rectangular filleted bar in tension or simple compression. $\sigma_0 = F/A$, where $A = dt$ and t is the thickness.

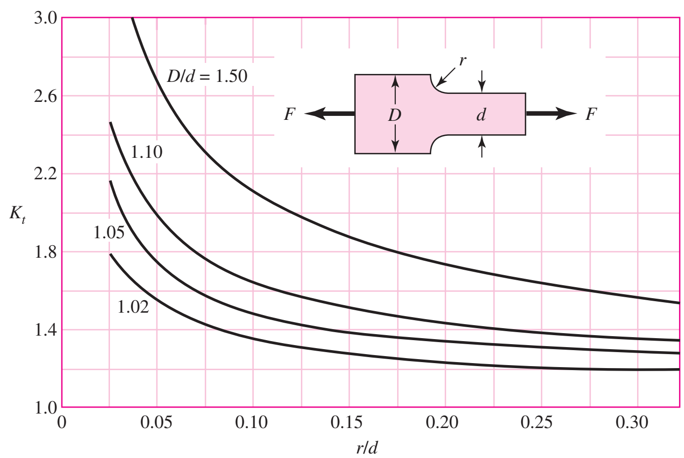

Figure A–15–6

Rectangular filleted bar in bending. $\sigma_0 = Mc/I$, where $c = d/2$, $I = td^3/12$, t is the thickness.

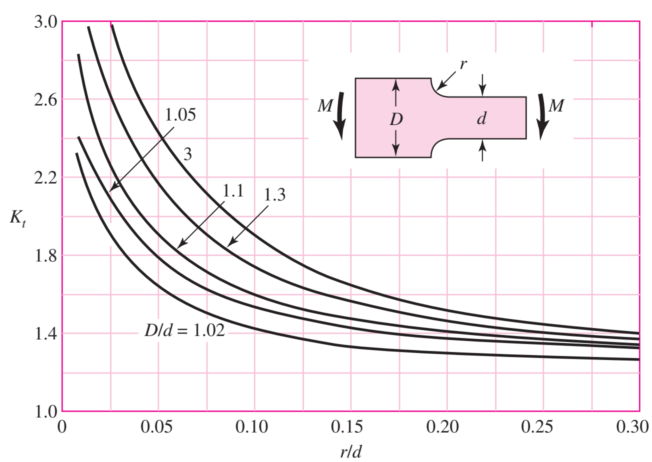

(continued)

*Factors from R. E. Peterson, "Design Factors for Stress Concentration," Machine Design, vol. 23, no. 2, February 1951, p. 169; no. 3, March 1951, p. 161, no. 5, May 1951, p. 159; no. 6, June 1951, p. 173; no. 7, July 1951, p. 155. Reprinted with permission from Machine Design, a Penton Media Inc. publication.

Table A–15

Charts of Theoretical Stress-Concentration Factors K_t^* *(Continued)*

Figure A–15–7

Round shaft with shoulder fillet in tension. $\sigma_0 = F/A$, where $A = \pi d^2/4$.

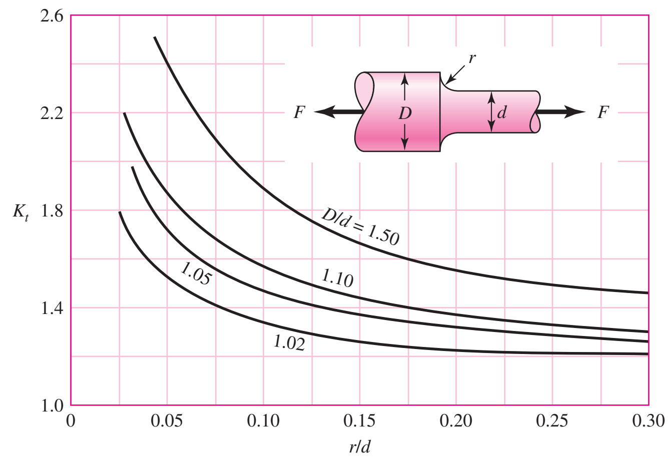

Figure A–15–8

Round shaft with shoulder fillet in torsion. $\tau_0 = Tc/J$, where $c = d/2$ and $J = \pi d^4/32$.

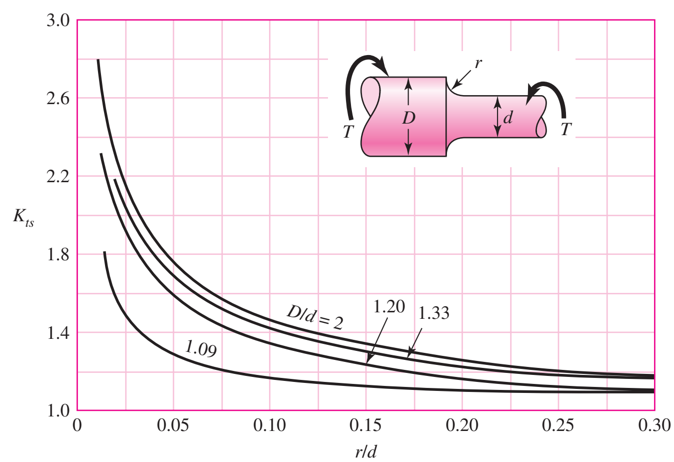

Figure A–15–9

Round shaft with shoulder fillet in bending. $\sigma_0 = Mc/I$, where $c = d/2$ and $I = \pi d^4/64$.

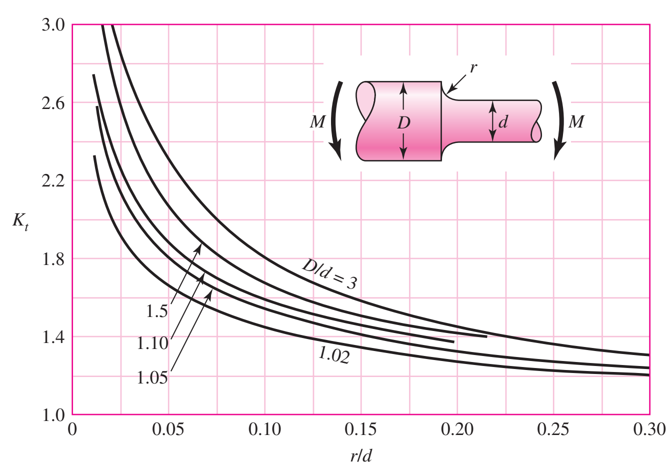

Table A–15

Charts of Theoretical Stress-Concentration Factors K_t^* *(Continued)*

Figure A–15–10

Round shaft in torsion with transverse hole.

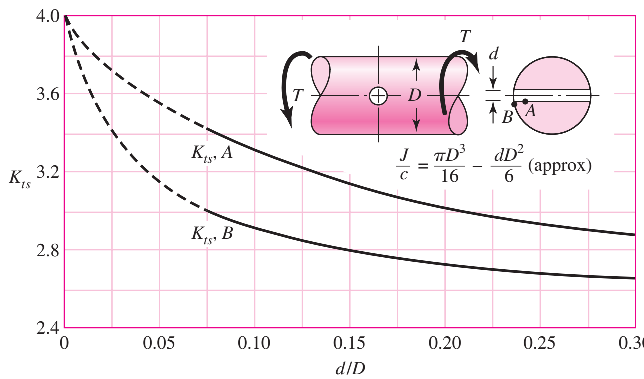

Figure A–15–11

Round shaft in bending with a transverse hole. $\sigma_0 = M/[(\pi D^3/32) - (dD^2/6)]$, approximately.

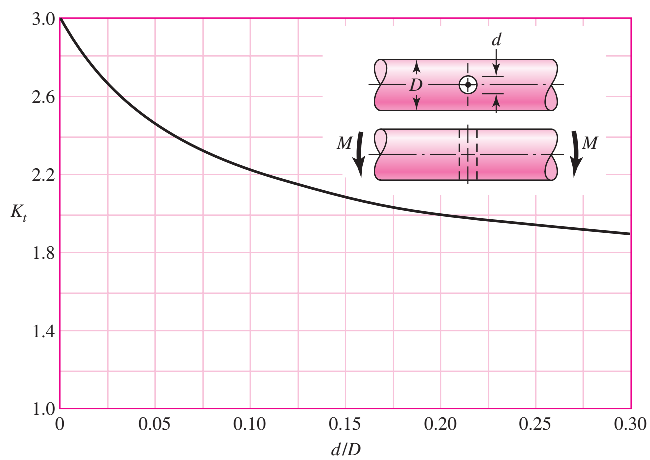

Figure A–15–12

Plate loaded in tension by a pin through a hole. $\sigma_0 = F/A$, where $A = (w - d)t$. When clearance exists, increase K_t 35 to 50 percent. *(M. M. Frocht and H. N. Hill, "Stress-Concentration Factors around a Central Circular Hole in a Plate Loaded through a Pin in Hole," J. Appl. Mechanics, vol. 7, no. 1, March 1940, p. A-5.)*

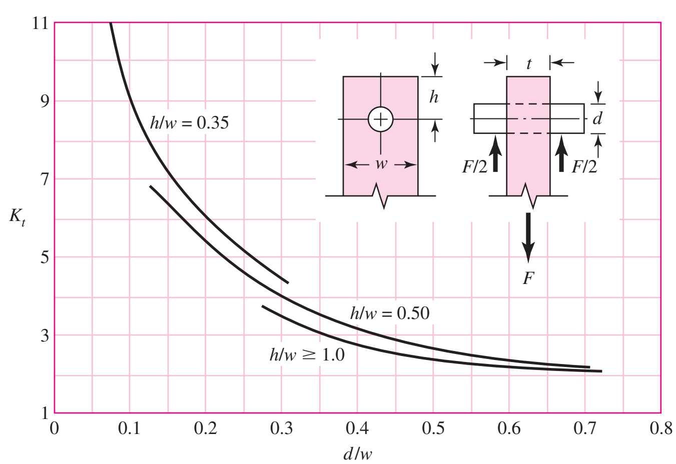

(continued)

*Factors from R. E. Peterson, "Design Factors for Stress Concentration," Machine Design, vol. 23, no. 2, February 1951, p. 169; no. 3, March 1951, p. 161, no. 5, May 1951, p. 159; no. 6, June 1951, p. 173; no. 7, July 1951, p. 155. Reprinted with permission from Machine Design, a Penton Media Inc. publication.

Table A–15

Charts of Theoretical Stress-Concentration Factors K_t^* *(Continued)*

Figure A–15–13

Grooved round bar in tension.
$\sigma_0 = F/A$, where $A = \pi d^2/4$.

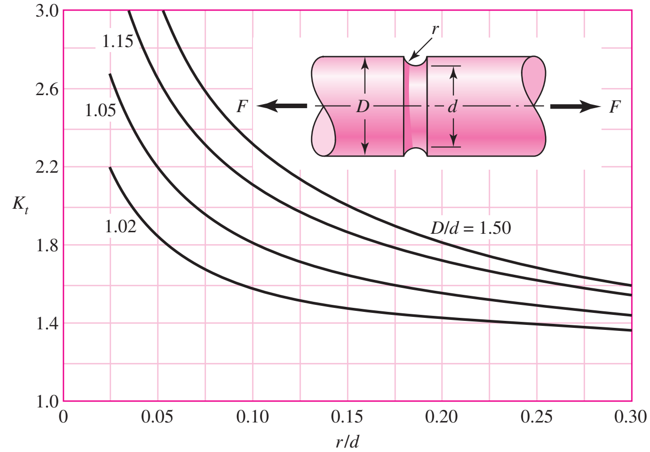

Figure A–15–14

Grooved round bar in bending.
$\sigma_0 = Mc/I$, where $c = d/2$ and $I = \pi d^4/64$.

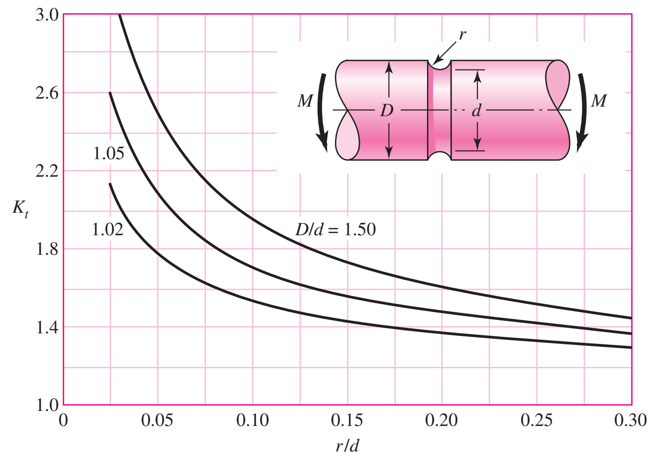

Figure A–15–15

Grooved round bar in torsion.
$\tau_0 = Tc/J$, where $c = d/2$ and $J = \pi d^4/32$.

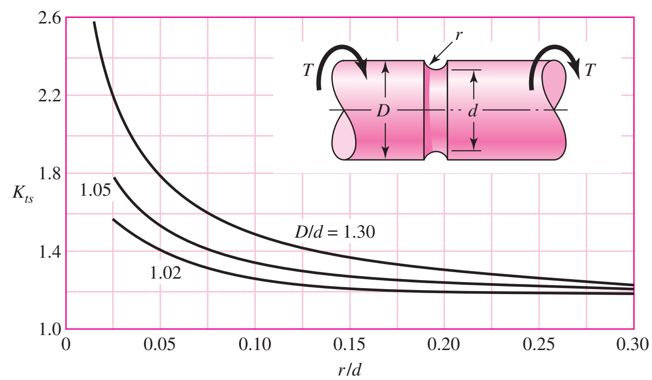

*Factors from R. E. Peterson, "Design Factors for Stress Concentration," Machine Design, vol. 23, no. 2, February 1951, p. 169; no. 3, March 1951, p. 161, no. 5, May 1951, p. 159; no. 6, June 1951, p. 173; no. 7, July 1951, p. 155. Reprinted with permission from Machine Design, a Penton Media Inc. publication.

Table A–15

Charts of Theoretical Stress-Concentration Factors K_t^* *(Continued)*

Figure A–15–16

Round shaft with flat-bottom groove in bending and/or tension.

$$\sigma_0 = \frac{4F}{\pi d^2} + \frac{32M}{\pi d^3}$$

Source: W. D. Pilkey, *Peterson's Stress-Concentration Factors,* 2nd ed. John Wiley & Sons, New York, 1997, p. 115.

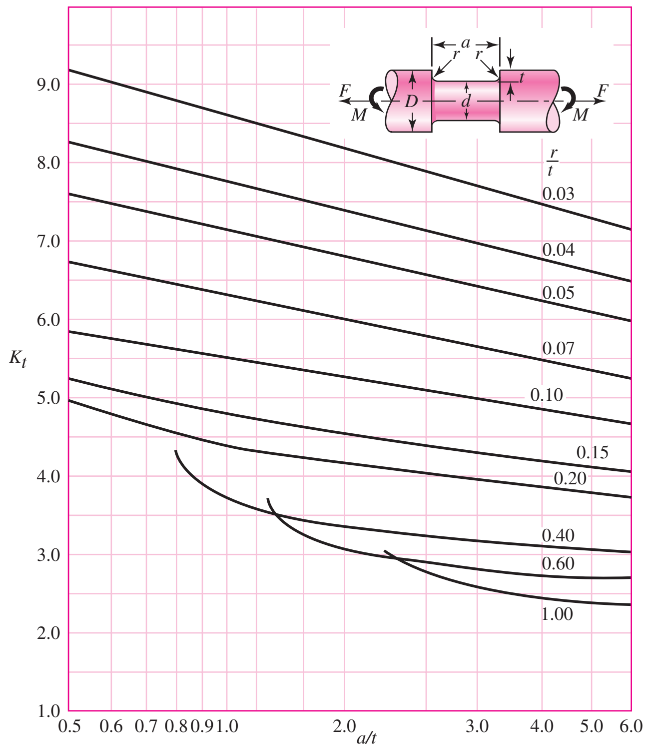

(continued)

Table A–15

Charts of Theoretical Stress-Concentration Factors K_t^* *(Continued)*

Figure A–15–17

Round shaft with flat-bottom groove in torsion.

$$\tau_0 = \frac{16T}{\pi d^3}$$

Source: W. D. Pilkey, *Peterson's Stress-Concentration Factors,* 2nd ed. John Wiley & Sons, New York, 1997, p. 133

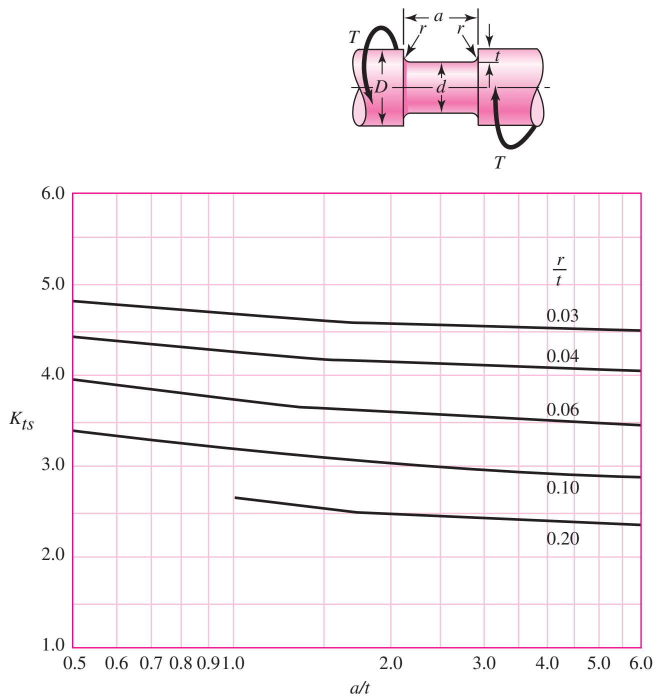

Table A–16

Approximate Stress-Concentration Factor K_t for Bending of a Round Bar or Tube with a Transverse Round Hole

Source: R. E. Peterson, *Stress-Concentration Factors,* Wiley, New York, 1974, pp. 146, 235.

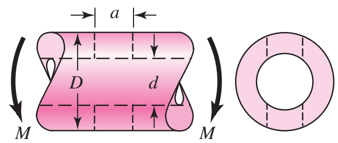

The nominal bending stress is $\sigma_0 = M/Z_{\text{net}}$ where Z_{net} is a reduced value of the section modulus and is defined by

$$Z_{\text{net}} = \frac{\pi A}{32D}(D^4 - d^4)$$

Values of A are listed in the table. Use $d = 0$ for a solid bar

	d/D					
	0.9		0.6		0	
a/D	A	K_t	A	K_t	A	K_t
0.050	0.92	2.63	0.91	2.55	0.88	2.42
0.075	0.89	2.55	0.88	2.43	0.86	2.35
0.10	0.86	2.49	0.85	2.36	0.83	2.27
0.125	0.82	2.41	0.82	2.32	0.80	2.20
0.15	0.79	2.39	0.79	2.29	0.76	2.15
0.175	0.76	2.38	0.75	2.26	0.72	2.10
0.20	0.73	2.39	0.72	2.23	0.68	2.07
0.225	0.69	2.40	0.68	2.21	0.65	2.04
0.25	0.67	2.42	0.64	2.18	0.61	2.00
0.275	0.66	2.48	0.61	2.16	0.58	1.97
0.30	0.64	2.52	0.58	2.14	0.54	1.94

(continued)

Table A–16 *(Continued)*

Approximate Stress-Concentration Factors K_{ts} for a Round Bar or Tube Having a Transverse Round Hole and Loaded in Torsion *Source:* R. E. Peterson, *Stress-Concentration Factors,* Wiley, New York, 1974, pp. 148, 244.

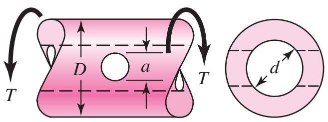

The maximum stress occurs on the inside of the hole, slightly below the shaft surface. The nominal shear stress is $\tau_0 = TD/2J_{\text{net}}$, where J_{net} is a reduced value of the second polar moment of area and is defined by

$$J_{\text{net}} = \frac{\pi A(D^4 - d^4)}{32}$$

Values of A are listed in the table. Use $d = 0$ for a solid bar.

	d/D									
	0.9		0.8		0.6		0.4		0	
a/D	A	K_{ts}	A	K_{ts}	A	K_{ts}	A	K_{ts}	A	K_{ts}
0.05	0.96	1.78							0.95	1.77
0.075	0.95	1.82							0.93	1.71
0.10	0.94	1.76	0.93	1.74	0.92	1.72	0.92	1.70	0.92	1.68
0.125	0.91	1.76	0.91	1.74	0.90	1.70	0.90	1.67	0.89	1.64
0.15	0.90	1.77	0.89	1.75	0.87	1.69	0.87	1.65	0.87	1.62
0.175	0.89	1.81	0.88	1.76	0.87	1.69	0.86	1.64	0.85	1.60
0.20	0.88	1.96	0.86	1.79	0.85	1.70	0.84	1.63	0.83	1.58
0.25	0.87	2.00	0.82	1.86	0.81	1.72	0.80	1.63	0.79	1.54
0.30	0.80	2.18	0.78	1.97	0.77	1.76	0.75	1.63	0.74	1.51
0.35	0.77	2.41	0.75	2.09	0.72	1.81	0.69	1.63	0.68	1.47
0.40	0.72	2.67	0.71	2.25	0.68	1.89	0.64	1.63	0.63	1.44

Table 6–3

$A_{0.95\sigma}$ Areas of Common Nonrotating Structural Shapes

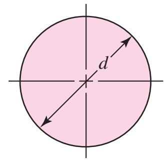

$$A_{0.95\sigma} = 0.01046d^2$$
$$d_e = 0.370d$$

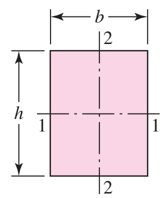

$$A_{0.95\sigma} = 0.05hb$$
$$d_e = 0.808\sqrt{hb}$$

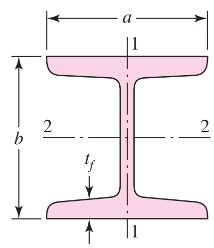

$$A_{0.95\sigma} = \begin{cases} 0.10at_f & & \text{axis 1-1} \\ 0.05ba & t_f > 0.025a & \text{axis 2-2} \end{cases}$$

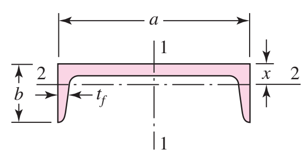

$$A_{0.95\sigma} = \begin{cases} 0.05ab & \text{axis 1-1} \\ 0.052xa + 0.1t_f(b - x) & \text{axis 2-2} \end{cases}$$

Loading Factor k_c

When fatigue tests are carried out with rotating bending, axial (push-pull), and torsional loading, the endurance limits differ with S_{ut}. This is discussed further in Sec. 6–17. Here, we will specify average values of the load factor as

$$k_c = \begin{cases} 1 & \text{bending} \\ 0.85 & \text{axial} \\ 0.59 & \text{torsion}^{17} \end{cases} \tag{6–26}$$

Temperature Factor k_d

When operating temperatures are below room temperature, brittle fracture is a strong possibility and should be investigated first. When the operating temperatures are higher than room temperature, yielding should be investigated first because the yield strength drops off so rapidly with temperature; see Fig. 2–9. Any stress will induce creep in a material operating at high temperatures; so this factor must be considered too.

[17]Use this only for pure torsional fatigue loading. When torsion is combined with other stresses, such as bending, $k_c = 1$ and the combined loading is managed by using the effective von Mises stress as in Sec. 5–5. *Note:* For pure torsion, the distortion energy predicts that $(k_c)_{\text{torsion}} = 0.577$.

Table 6–4

Effect of Operating Temperature on the Tensile Strength of Steel.* (S_T = tensile strength at operating temperature; S_{RT} = tensile strength at room temperature; $0.099 \leq \hat{\sigma} \leq 0.110$)

Temperature, °C	S_T/S_{RT}	Temperature, °F	S_T/S_{RT}
20	1.000	70	1.000
50	1.010	100	1.008
100	1.020	200	1.020
150	1.025	300	1.024
200	1.020	400	1.018
250	1.000	500	0.995
300	0.975	600	0.963
350	0.943	700	0.927
400	0.900	800	0.872
450	0.843	900	0.797
500	0.768	1000	0.698
550	0.672	1100	0.567
600	0.549		

*Data source: Fig. 2–9.

Finally, it may be true that there is no fatigue limit for materials operating at high temperatures. Because of the reduced fatigue resistance, the failure process is, to some extent, dependent on time.

The limited amount of data available show that the endurance limit for steels increases slightly as the temperature rises and then begins to fall off in the 400 to 700°F range, not unlike the behavior of the tensile strength shown in Fig. 2–9. For this reason it is probably true that the endurance limit is related to tensile strength at elevated temperatures in the same manner as at room temperature.[18] It seems quite logical, therefore, to employ the same relations to predict endurance limit at elevated temperatures as are used at room temperature, at least until more comprehensive data become available. At the very least, this practice will provide a useful standard against which the performance of various materials can be compared.

Table 6–4 has been obtained from Fig. 2–9 by using only the tensile-strength data. Note that the table represents 145 tests of 21 different carbon and alloy steels. A fourth-order polynomial curve fit to the data underlying Fig. 2–9 gives

$$\begin{aligned} k_d = 0.975 &+ 0.432(10^{-3})T_F - 0.115(10^{-5})T_F^2 \\ &+ 0.104(10^{-8})T_F^3 - 0.595(10^{-12})T_F^4 \end{aligned} \tag{6–27}$$

where $70 \leq T_F \leq 1000°\text{F}$.

Two types of problems arise when temperature is a consideration. If the rotating-beam endurance limit is known at room temperature, then use

$$k_d = \frac{S_T}{S_{RT}} \tag{6–28}$$

[18]For more, see Table 2 of ANSI/ASME B106. 1M-1985 shaft standard, and E. A. Brandes (ed.), *Smithell's Metals Reference Book,* 6th ed., Butterworth, London, 1983, pp. 22–134 to 22–136, where endurance limits from 100 to 650°C are tabulated.

Table 6–5

Reliability Factors k_e Corresponding to 8 Percent Standard Deviation of the Endurance Limit

Reliability, %	Transformation Variate z_a	Reliability Factor k_e
50	0	1.000
90	1.288	0.897
95	1.645	0.868
99	2.326	0.814
99.9	3.091	0.753
99.99	3.719	0.702
99.999	4.265	0.659
99.9999	4.753	0.620

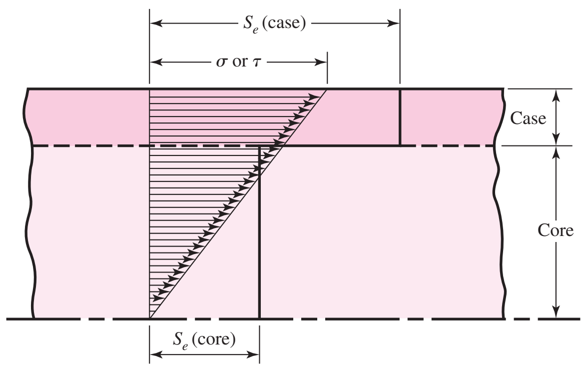

Figure 6–19

The failure of a case-hardened part in bending or torsion. In this example, failure occurs in the core.

Miscellaneous-Effects Factor k_f

Though the factor k_f is intended to account for the reduction in endurance limit due to all other effects, it is really intended as a reminder that these must be accounted for, because actual values of k_f are not always available.

Residual stresses may either improve the endurance limit or affect it adversely. Generally, if the residual stress in the surface of the part is compression, the endurance limit is improved. Fatigue failures appear to be tensile failures, or at least to be caused by tensile stress, and so anything that reduces tensile stress will also reduce the possibility of a fatigue failure. Operations such as shot peening, hammering, and cold rolling build compressive stresses into the surface of the part and improve the endurance limit significantly. Of course, the material must not be worked to exhaustion.

The endurance limits of parts that are made from rolled or drawn sheets or bars, as well as parts that are forged, may be affected by the so-called *directional characteristics* of the operation. Rolled or drawn parts, for example, have an endurance limit in the transverse direction that may be 10 to 20 percent less than the endurance limit in the longitudinal direction.

Parts that are case-hardened may fail at the surface or at the maximum core radius, depending upon the stress gradient. Figure 6–19 shows the typical triangular stress distribution of a bar under bending or torsion. Also plotted as a heavy line in this figure are the endurance limits S_e for the case and core. For this example the endurance limit of the core rules the design because the figure shows that the stress σ or τ, whichever applies, at the outer core radius, is appreciably larger than the core endurance limit.

6–10 Stress Concentration and Notch Sensitivity

In Sec. 3–13 it was pointed out that the existence of irregularities or discontinuities, such as holes, grooves, or notches, in a part increases the theoretical stresses significantly in the immediate vicinity of the discontinuity. Equation (3–48) defined a stress-concentration factor K_t (or K_{ts}), which is used with the nominal stress to obtain the maximum resulting stress due to the irregularity or defect. It turns out that some materials are not fully sensitive to the presence of notches and hence, for these, a reduced value of K_t can be used. For these materials, the effective maximum stress in fatigue is,

$$\sigma_{\max} = K_f \sigma_0 \qquad \text{or} \qquad \tau_{\max} = K_{fs} \tau_0 \tag{6–30}$$

where K_f is a reduced value of K_t and σ_0 is the nominal stress. The factor K_f is commonly called a *fatigue stress-concentration factor,* and hence the subscript *f*. So it is convenient to think of K_f as a stress-concentration factor reduced from K_t because of lessened sensitivity to notches. The resulting factor is defined by the equation

$$K_f = \frac{\text{maximum stress in notched specimen}}{\text{stress in notch-free specimen}} \tag{a}$$

Notch sensitivity q is defined by the equation

$$q = \frac{K_f - 1}{K_t - 1} \qquad \text{or} \qquad q_{\text{shear}} = \frac{K_{fs} - 1}{K_{ts} - 1} \tag{6–31}$$

where q is usually between zero and unity. Equation (6–31) shows that if $q = 0$, then $K_f = 1$, and the material has no sensitivity to notches at all. On the other hand, if $q = 1$, then $K_f = K_t$, and the material has full notch sensitivity. In analysis or design work, find K_t first, from the geometry of the part. Then specify the material, find q, and solve for K_f from the equation

$$K_f = 1 + q(K_t - 1) \qquad \text{or} \qquad K_{fs} = 1 + q_{\text{shear}}(K_{ts} - 1) \tag{6–32}$$

Notch sensitivities for specific materials are obtained experimentally. Published experimental values are limited, but some values are available for steels and aluminum. Trends for notch sensitivity as a function of notch radius and ultimate strength are shown in Fig. 6–20 for reversed bending or axial loading, and Fig. 6–21 for reversed

Figure 6–20

Notch-sensitivity charts for steels and UNS A92024-T wrought aluminum alloys subjected to reversed bending or reversed axial loads. For larger notch radii, use the values of q corresponding to the $r = 0.16$-in (4-mm) ordinate. *(From George Sines and J. L. Waisman (eds.),* Metal Fatigue, *McGraw-Hill, New York. Copyright © 1969 by The McGraw-Hill Companies, Inc. Reprinted by permission.)*

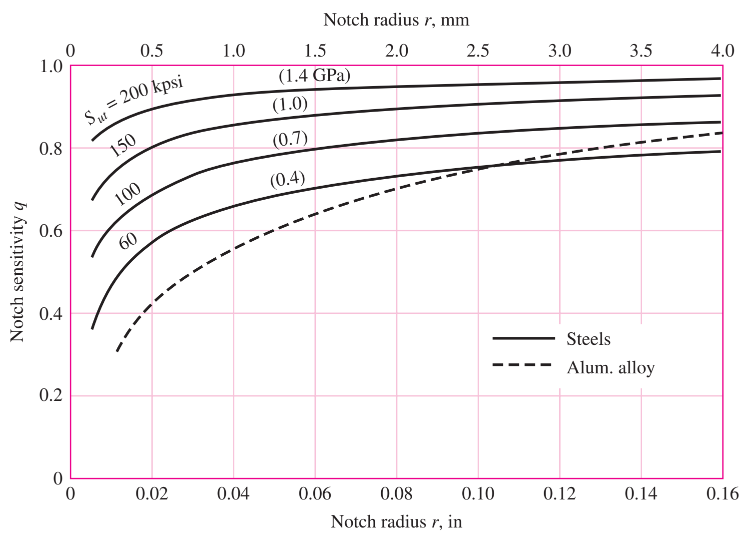

Figure 6–21

Notch-sensitivity curves for materials in reversed torsion. For larger notch radii, use the values of q_{shear} corresponding to $r = 0.16$ in (4 mm).

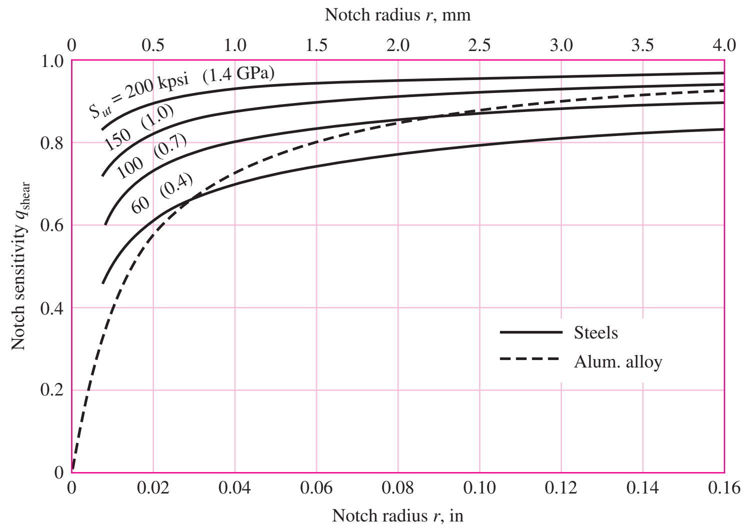

torsion. In using these charts it is well to know that the actual test results from which the curves were derived exhibit a large amount of scatter. Because of this scatter it is always safe to use $K_f = K_t$ if there is any doubt about the true value of q. Also, note that q is not far from unity for large notch radii.

Figure 6–20 has as its basis the *Neuber equation,* which is given by

$$K_f = 1 + \frac{K_t - 1}{1 + \sqrt{a/r}} \tag{6–33}$$

where $\sqrt{a}$ is defined as the *Neuber constant* and is a material constant. Equating Eqs. (6–31) and (6–33) yields the notch sensitivity equation

$$q = \frac{1}{1 + \dfrac{\sqrt{a}}{\sqrt{r}}} \tag{6–34}$$

correlating with Figs. 6–20 and 6–21 as

Bending or axial: $\sqrt{a} = 0.246 - 3.08(10^{-3})S_{ut} + 1.51(10^{-5})S_{ut}^2 - 2.67(10^{-8})S_{ut}^3$ (6–35*a*)

Torsion: $\sqrt{a} = 0.190 - 2.51(10^{-3})S_{ut} + 1.35(10^{-5})S_{ut}^2 - 2.67(10^{-8})S_{ut}^3$ (6–35*b*)

where the equations apply to steel and S_{ut} is in kpsi. Equation (6–34) used in conjunction with Eq. pair (6–35) is equivalent to Figs. (6–20) and (6–21). As with the graphs, the results from the curve fit equations provide only approximations to the experimental data.

The notch sensitivity of cast irons is very low, varying from 0 to about 0.20, depending upon the tensile strength. To be on the conservative side, it is recommended that the value $q = 0.20$ be used for all grades of cast iron.

EXAMPLE 6–6

A steel shaft in bending has an ultimate strength of 690 MPa and a shoulder with a fillet radius of 3 mm connecting a 32-mm diameter with a 38-mm diameter. Estimate K_f using:
(*a*) Figure 6–20.
(*b*) Equations (6–33) and (6–35).

مثال: در شکل روبرو اگر بخواهیم $b=2t$ باشد با استفاده از معیار ترسکا، ابعاد b و t را طوری بیابید که ماکزیمم تنش در عضو از 60 MPa تجاوز نکند.

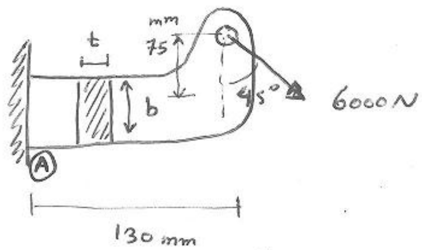

خطرناک‌ترین مقطع، مقطع A است.

نیروی 6000 نیوتنی را به سطح مقطع در مقطع A منتقل می‌کنیم.

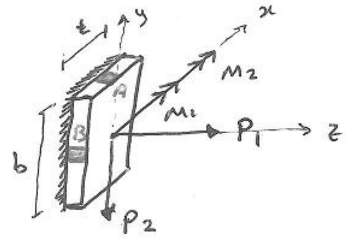

$$P_1 = 6000 \times \sin 45^\circ = 4.24 \text{ kN}$$

$$P_2 = 6000 \times \cos 45^\circ = 4.24 \text{ kN}$$

$$M_1 = 6000 \times \sin 45^\circ \times 75\times 10^{-3} = 318.2 \text{ N.m}$$

$$M_2 = 6000 \times \cos 45^\circ \times 130\times 10^{-3} = 551.5 \text{ N.m}$$

$$M_t = M_1 + M_2 = 318.2 + 551.5 = 869.7 \text{ N.m}$$

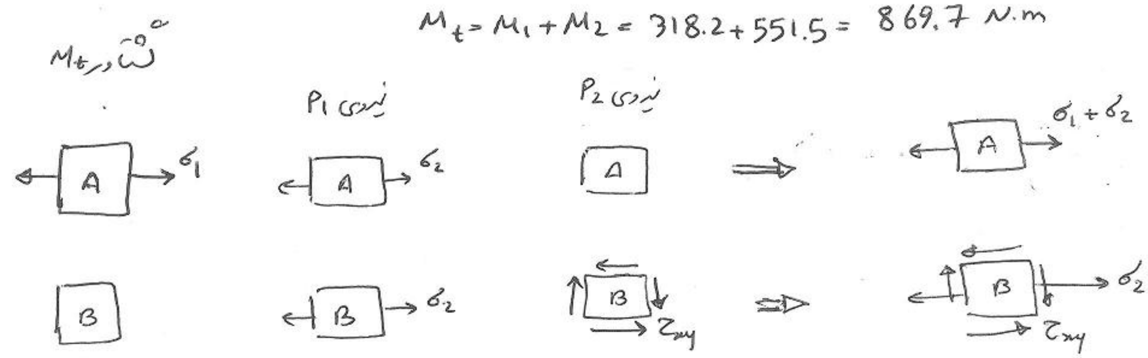

$$\sigma_1 = \frac{m.C}{I} = \frac{869.7 \times (2t)\times 12}{2\times t\times (2t)^3} = \frac{1304.55}{t^3}$$

$$\sigma_2 = \frac{P_1}{A} = \frac{4.24\times 10^3}{t\times (2t)} = \frac{2.12\times 10^3}{t^2}$$

$$\tau = \frac{3}{2}\frac{V}{A} = \frac{3\times 4.24\times 10^3}{2\times t\times (2t)} = \frac{3.180\times 10^3}{t^2}$$

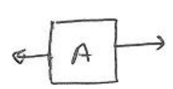

$$\sigma = \sigma_1 + \sigma_2 = \frac{1304.55}{t^3} + \frac{2.12\times 10^3}{t^2} = \sigma_{max}$$

با ترسکا: $\frac{1304.55}{t^3} + \frac{2.12\times 10^3}{t^2} = S_y = 60 \text{ MPa} \longrightarrow t = 0.0286 \quad b = 0.0572$

$t = 28.6 \text{ mm} \quad b = 57.2$

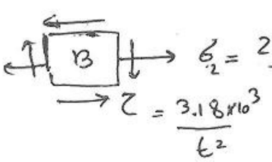

$$\sigma_2 = \frac{2.12\times 10^3}{t^2}, \quad \tau = \frac{3.18\times 10^3}{t^2} \longrightarrow \tau_{max} = \sqrt{\left(\frac{2.12\times 10^3}{2\times t^2}\right)^2 + \left(\frac{3.18\times 10^3}{t^2}\right)^2} = \frac{3352}{t^2}$$

$$\tau_{max} = \frac{S_y}{2} \Rightarrow \frac{3352}{t^2} = \frac{60\times 10^6}{2} \Rightarrow t = 0.0105 \text{ m} \Rightarrow t = 10.57 \text{ mm} \quad b = 21.14 \text{ mm}$$

بر اساس تحلیل فوق برای المان‌های A، B در نهایت ابعاد زیر انتخاب می‌شود:

$t = 28.6 \text{ mm} \quad b = 57.2 \text{ mm}$

مثال ۲: اگر شافت زیر در حالت استاتیک قرار داشته باشد با در نظر گرفتن ضریب اطمینان 2 در صورتی که جنس شافت دارای تنش تسلیم $\sigma_y = 350$ MPa باشد، حداکثر مقدار مجاز a را براساس تئوری تنش بیابید.

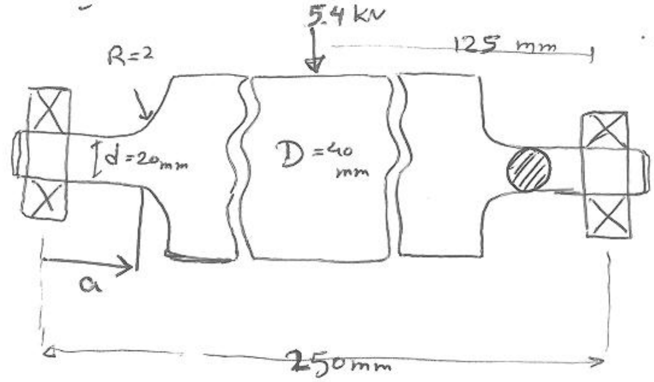

$$M_1 = 2.7 \times 10^3 \times 125 \times 10^{-3} = 337.5\ N.m$$

$$M_2 = 2.7 \times 10^3 \times a$$

$$\left.\begin{aligned} r/d &= \frac{2}{20} = 0.1 \\ \frac{D}{d} &= \frac{40}{20} = 2 \end{aligned}\right\} \Rightarrow K_t = 1.7$$ ضریب تمرکز تنش

با استفاده از نمودارهای کتاب

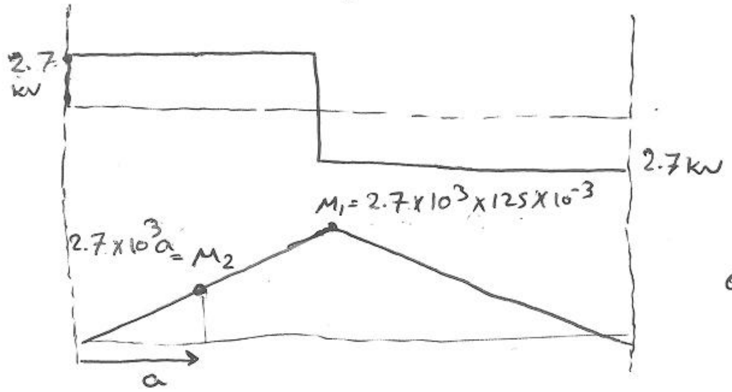

$$S_{all} = \frac{S_y}{\underset{n}{2}} = \frac{350}{2}$$

$$\sigma = \frac{M.C}{I} = \frac{2.7 \times 10^3 \times a \times 0.01 \times 4}{\pi \times (0.01)^4} = 3437.7 \times 10^6 \times a$$

$$\sigma_d = \sigma \times K_t = 3437.7 \times 10^6 \times a \times 1.7 = 5844.17 \times 10^6 \times a$$ طراحی

$$\sigma_d = \frac{S_y}{2} \longrightarrow 5844.17 \times 10^6 \times a = \frac{350 \times 10^6}{2} \Rightarrow a = 0.03\ m$$

$$a = 30\ mm$$

تنش در نقطه زیر ماکزیمم خمش «جهت چک»:

$$\sigma = \frac{M.C}{I} = \frac{337.5 \times 0.02 \times 4}{\pi \times (0.02)^4} = 53.7\ MPa$$

ضریب اطمینان این نقطه برابر است با:

$$n = \frac{350}{53.7} = 6.5$$

لذا نقطه بحرانی نقطه زیر a می‌باشد.

مثال ۱۰: ضریب اطمینان را براساس تئوری انرژی واپیچش و تئوری ترسکا برای شکل مقابل بیابید
نقاط A, B

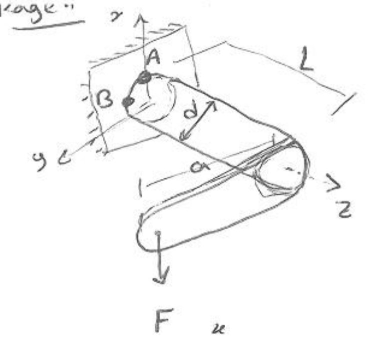

$d = 4\,cm \quad ; \quad L = 15\,cm$

$F = 500\,kg \quad ; \quad a = 20\,cm$

$S_y = 230\,MPa \rightarrow \tau_y = \frac{230}{2} = 115\,MPa$

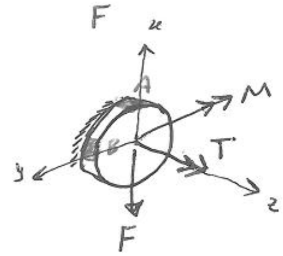

$F = 500 \times 9.81 = 4.9\,kN$

$T = 500 \times 9.81 \times 20 \times 10^{-2} = 981\,N.m$

$M = 500 \times 9.81 \times 15 \times 10^{-2} = 735.75\,N.m$

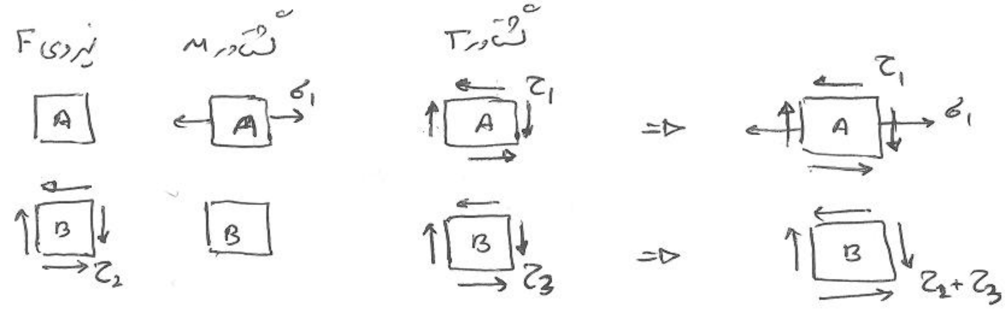

$$\sigma_1 = \frac{m.c}{I} = \frac{735.75 \times 2\times10^{-2} \times 4}{\pi \times (2\times10^{-2})^4} = 117.1\,MPa$$

$$\tau_3 = \tau_1 = \frac{T.c}{J} = \frac{981 \times 2\times10^{-2} \times 2}{\pi \times (2\times10^{-2})^4} = 78.1\,MPa \qquad \tau_2 = \frac{4}{3}\frac{V}{A} = \frac{4 \times 4.9 \times 10^3}{3 \times \pi \times (2\times10^{-2})^2} = 5.2\,MPa$$

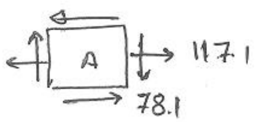

$\sigma_x = 117.1$

$\tau_{xy} = 78.1$

$$\tau_{max} = \sqrt{\left(\frac{117.1}{2}\right)^2 + 78.1^2} = 97.6\,MPa \qquad \text{ترسکا}: \; n = \frac{115}{97.6} = \boxed{1.178}$$

فن مایزز $\left[117.1^2 + 3 \times 78.1^2\right]^{1/2} = \frac{S_y}{n} = \frac{230}{n} \Rightarrow \boxed{n = 1.285}$ فن مایزز

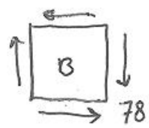

$78.1 + 5.2 = 83.3\,MPa \quad ; \quad \tau_{max} = 83.3\,MPa$

ترسکا: $n = \frac{115}{83.3} = 1.38$

فن مایزز $\left[3 \times 83.3^2\right]^{1/2} = \frac{S_y}{n} = \frac{230}{n} \Rightarrow n = 1.59$

ملاحظه می‌گردد که ضریب اطمینان با استفاده از تئوری فن مایزز بیشتر بدست می‌آید (برای هر دو حالت) و لذا تئوری ترسکا محافظه‌کارانه است. همچنین نقطه A از نقطه B دارای ضریب اطمینان کمتری است و لذا خطرناک‌تر است.

مثال: در شکل زیر با در نظر گرفتن ضریب اطمینان 2، حداقل تنش کشش جاری شدن باید چقدر باشد تا قطعه تحمل نیروی وارد شده را داشته باشد.

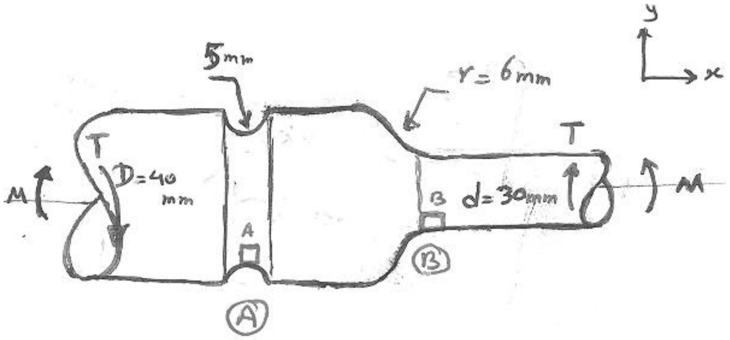

کوپل خمشی M حول محور z بوده و مقدار آن برابر $300^{N.m}$

و کوپل پیچشی T حول محور x بوده و مقدار آن برابر $500^{N.m}$

می باشد. معیار مورد نظر فون مایزز می باشد.

مقطع B برای شافت پله دار:

$$\text{خمش} \rightarrow \frac{r}{d} = \frac{6}{30} = 0.2 \ ; \ \frac{D}{d} = 1.33 \Rightarrow k_t = 1.4 \quad \text{Figure - A-15-9}$$

$$\text{پیچش} \rightarrow r/d = 0.2 \ ; \ \frac{D}{d} = 1.33 \Rightarrow k_{ts} = 1.22 \quad \text{Figure - A-15-8}$$

مقطع A برای شافت شیار دار:

$$\text{خمش} \rightarrow r/d = \frac{5}{40} = 0.125 \ ; \ \frac{D}{d} = \frac{40}{40-10} = 1.33 \Rightarrow k_t = 1.8 \quad \text{Figure-A-15-14}$$

$$\text{پیچش} \rightarrow r/d = 0.125 \ ; \ \frac{D}{d} = \frac{40}{30} = 1.33 \Rightarrow k_{ts} = 1.42 \quad \text{Figure A-15-15}$$

در مقطع A:
المان A

$$\text{خمش} \Rightarrow \sigma_0 = \frac{m.c}{I} = \frac{300 \times (40-10) \times 10^{-3} \times 4}{2 \times \pi \times (15 \times 10^{-3})^4} = 113.18 \text{ MPa}$$

$$\sigma_{max} = \sigma_0 \times k_t = 113.18 \times 1.8 = 203.7 \text{ MPa}$$

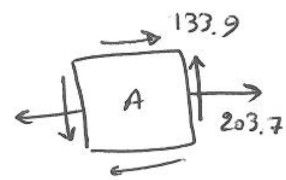

$$\text{پیچش} \Rightarrow \tau_0 = \frac{T.c}{J} = \frac{500 \times 15 \times 10^{-3} \times 2}{\pi \times (15 \times 10^{-3})^4} = 94.3 \text{ MPa}$$

$$\tau_{max} = \tau_0 \times k_{ts} = 94.3 \times 1.42 = 133.9 \text{ MPa}$$

فون مایزز:

$$\left[203.7^2 + 3 \times 133.9^2\right]^{1/2} = \frac{S_y}{\underset{2}{n}} \Rightarrow \boxed{S_y = 617.35 \text{ MPa}}$$

در مقطع B:
المان B

$$\text{خمش} \rightarrow \sigma_0 = \frac{m.c}{I} = \frac{300 \times 15 \times 10^{-3} \times 4}{\pi \times (15 \times 10^{-3})^4} = 113.18 \text{ MPa}$$

$$\sigma_{max} = \sigma_0 \times k_t = 113.18 \times 1.4 = 158.5 \text{ MPa}$$

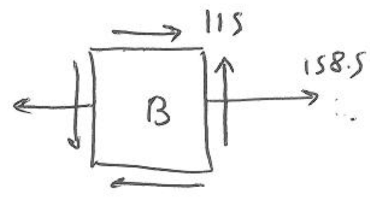

$$\text{پیچش} \rightarrow \tau_0 = \frac{T.c}{J} = \frac{500 \times 15 \times 10^{-3} \times 2}{\pi \times (15 \times 10^{-3})^4} = 94.3 \text{ MPa}$$

$$\tau_{max} = \tau_0 \times k_{ts} = 94.3 \times 1.22 = 115 \text{ MPa}$$

فون مایزز:

$$\left[158.5^2 + 3 \times 115^2\right]^{1/2} = \frac{S_y}{\underset{2}{n}} \Rightarrow S_y = 400 \text{ MPa}$$

جنس قطعه باید تنش تسلیم آن از 617.35 MPa بیشتر باشد. و مقطع A خطرناک تر است.

Combining these stresses in accordance with the distortion energy failure theory, the von Mises stresses for rotating round, solid shafts, neglecting axial loads, are given by

$$\sigma_a' = (\sigma_a^2 + 3\tau_a^2)^{1/2} = \left[\left(\frac{32K_f M_a}{\pi d^3}\right)^2 + 3\left(\frac{16K_{fs}T_a}{\pi d^3}\right)^2\right]^{1/2} \tag{7–5}$$

$$\sigma_m' = (\sigma_m^2 + 3\tau_m^2)^{1/2} = \left[\left(\frac{32K_f M_m}{\pi d^3}\right)^2 + 3\left(\frac{16K_{fs}T_m}{\pi d^3}\right)^2\right]^{1/2} \tag{7–6}$$

Note that the stress-concentration factors are sometimes considered optional for the midrange components with ductile materials, because of the capacity of the ductile material to yield locally at the discontinuity.

These equivalent alternating and midrange stresses can be evaluated using an appropriate failure curve on the modified Goodman diagram (See Sec. 6–12, p. 303, and Fig. 6–27). For example, the fatigue failure criteria for the modified Goodman line as expressed previously in Eq. (6–46) is

$$\frac{1}{n} = \frac{\sigma_a'}{S_e} + \frac{\sigma_m'}{S_{ut}}$$

Substitution of σ_a' and σ_m' from Eqs. (7–5) and (7–6) results in

$$\frac{1}{n} = \frac{16}{\pi d^3}\left\{\frac{1}{S_e}\left[4(K_f M_a)^2 + 3(K_{fs}T_a)^2\right]^{1/2} + \frac{1}{S_{ut}}\left[4(K_f M_m)^2 + 3(K_{fs}T_m)^2\right]^{1/2}\right\}$$

For design purposes, it is also desirable to solve the equation for the diameter. This results in

$$d = \left(\frac{16n}{\pi}\left\{\frac{1}{S_e}\left[4(K_f M_a)^2 + 3(K_{fs}T_a)^2\right]^{1/2} + \frac{1}{S_{ut}}\left[4(K_f M_m)^2 + 3(K_{fs}T_m)^2\right]^{1/2}\right\}\right)^{1/3}$$

Similar expressions can be obtained for any of the common failure criteria by substituting the von Mises stresses from Eqs. (7–5) and (7–6) into any of the failure criteria expressed by Eqs. (6–45) through (6–48), p. 306. The resulting equations for several of the commonly used failure curves are summarized below. The names given to each set of equations identifies the significant failure theory, followed by a fatigue failure locus name. For example, DE-Gerber indicates the stresses are combined using the distortion energy (DE) theory, and the Gerber criteria is used for the fatigue failure.

DE-Goodman

$$\frac{1}{n} = \frac{16}{\pi d^3}\left\{\frac{1}{S_e}\left[4(K_f M_a)^2 + 3(K_{fs}T_a)^2\right]^{1/2} + \frac{1}{S_{ut}}\left[4(K_f M_m)^2 + 3(K_{fs}T_m)^2\right]^{1/2}\right\} \tag{7–7}$$

$$d = \left(\frac{16n}{\pi}\left\{\frac{1}{S_e}\left[4(K_f M_a)^2 + 3(K_{fs}T_a)^2\right]^{1/2} + \frac{1}{S_{ut}}\left[4(K_f M_m)^2 + 3(K_{fs}T_m)^2\right]^{1/2}\right\}\right)^{1/3} \tag{7–8}$$

DE-Gerber

$$\frac{1}{n} = \frac{8A}{\pi d^3 S_e}\left\{1 + \left[1 + \left(\frac{2BS_e}{AS_{ut}}\right)^2\right]^{1/2}\right\} \tag{7–9}$$

$$d = \left(\frac{8nA}{\pi S_e}\left\{1 + \left[1 + \left(\frac{2BS_e}{AS_{ut}}\right)^2\right]^{1/2}\right\}\right)^{1/3} \tag{7–10}$$

where

$$A = \sqrt{4(K_f M_a)^2 + 3(K_{fs}T_a)^2}$$

$$B = \sqrt{4(K_f M_m)^2 + 3(K_{fs}T_m)^2}$$

DE-ASME Elliptic

$$\frac{1}{n} = \frac{16}{\pi d^3}\left[4\left(\frac{K_f M_a}{S_e}\right)^2 + 3\left(\frac{K_{fs}T_a}{S_e}\right)^2 + 4\left(\frac{K_f M_m}{S_y}\right)^2 + 3\left(\frac{K_{fs}T_m}{S_y}\right)^2\right]^{1/2} \tag{7–11}$$

$$d = \left\{\frac{16n}{\pi}\left[4\left(\frac{K_f M_a}{S_e}\right)^2 + 3\left(\frac{K_{fs}T_a}{S_e}\right)^2 + 4\left(\frac{K_f M_m}{S_y}\right)^2 + 3\left(\frac{K_{fs}T_m}{S_y}\right)^2\right]^{1/2}\right\}^{1/3} \tag{7–12}$$

DE-Soderberg

$$\frac{1}{n} = \frac{16}{\pi d^3}\left\{\frac{1}{S_e}\left[4(K_f M_a)^2 + 3(K_{fs}T_a)^2\right]^{1/2} + \frac{1}{S_{yt}}\left[4(K_f M_m)^2 + 3(K_{fs}T_m)^2\right]^{1/2}\right\} \tag{7–13}$$

$$d = \left(\frac{16n}{\pi}\left\{\frac{1}{S_e}\left[4(K_f M_a)^2 + 3(K_{fs}T_a)^2\right]^{1/2} + \frac{1}{S_{yt}}\left[4(K_f M_m)^2 + 3(K_{fs}T_m)^2\right]^{1/2}\right\}\right)^{1/3} \tag{7–14}$$

For a rotating shaft with constant bending and torsion, the bending stress is completely reversed and the torsion is steady. Equations (7–7) through (7–14) can be simplified by setting M_m and T_a equal to 0, which simply drops out some of the terms.

Note that in an analysis situation in which the diameter is known and the factor of safety is desired, as an alternative to using the specialized equations above, it is always still valid to calculate the alternating and mid-range stresses using Eqs. (7–5) and (7–6), and substitute them into one of the equations for the failure criteria, Eqs. (6–45) through (6–48), and solve directly for n. In a design situation, however, having the equations pre-solved for diameter is quite helpful.

It is always necessary to consider the possibility of static failure in the first load cycle. The Soderberg criteria inherently guards against yielding, as can be seen by noting that its failure curve is conservatively within the yield (Langer) line on Fig. 6–27, p. 305. The ASME Elliptic also takes yielding into account, but is not entirely conservative

Figure 10–2

Types of ends for compression springs: (*a*) both ends plain; (*b*) both ends squared; (*c*) both ends squared and ground; (*d*) both ends plain and ground.

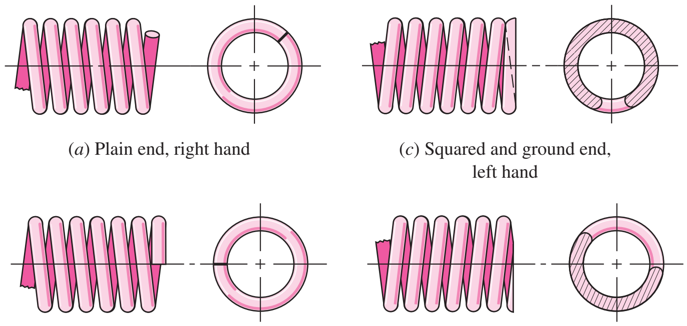

(*a*) Plain end, right hand

(*c*) Squared and ground end, left hand

(*b*) Squared or closed end, right hand

(*d*) Plain end, ground, left hand

Table 10–1

Formulas for the Dimensional Characteristics of Compression-Springs. (N_a = Number of Active Coils)

Source: From *Design Handbook,* 1987, p. 32. Courtesy of Associated Spring.

	Type of Spring Ends			
Term	**Plain**	**Plain and Ground**	**Squared or Closed**	**Squared and Ground**
End coils, N_e	0	1	2	2
Total coils, N_t	N_a	$N_a + 1$	$N_a + 2$	$N_a + 2$
Free length, L_0	$pN_a + d$	$p(N_a + 1)$	$pN_a + 3d$	$pN_a + 2d$
Solid length, L_s	$d(N_t + 1)$	dN_t	$d(N_t + 1)$	dN_t
Pitch, p	$(L_0 - d)/N_a$	$L_0/(N_a + 1)$	$(L_0 - 3d)/N_a$	$(L_0 - 2d)/N_a$

used without question. *Some of these need closer scrutiny as they may not be integers.* This depends on how a springmaker forms the ends. Forys[4] pointed out that squared and ground ends give a solid length L_s of

$$L_s = (N_t - a)d$$

where a varies, with an average of 0.75, so the entry dN_t in Table 10–1 may be overstated. The way to check these variations is to take springs from a particular springmaker, close them solid, and measure the solid height. Another way is to look at the spring and count the wire diameters in the solid stack.

Set removal or *presetting* is a process used in the manufacture of compression springs to induce useful residual stresses. It is done by making the spring longer than needed and then compressing it to its solid height. This operation *sets* the spring to the required final free length and, since the torsional yield strength has been exceeded, induces residual stresses opposite in direction to those induced in service. Springs to be preset should be designed so that 10 to 30 percent of the initial free length is removed during the operation. If the stress at the solid height is greater than 1.3 times the torsional yield strength, distortion may occur. If this stress is much less than 1.1 times, it is difficult to control the resulting free length.

Set removal increases the strength of the spring and so is especially useful when the spring is used for energy-storage purposes. However, set removal should not be used when springs are subject to fatigue.

[4]Edward L. Forys, "Accurate Spring Heights," *Machine Design,* vol. 56, no. 2, January 26, 1984.

10–5 Stability

In Chap. 4 we learned that a column will buckle when the load becomes too large. Similarly, compression coil springs may buckle when the deflection becomes too large. The critical deflection is given by the equation

$$y_{cr} = L_0 C'_1 \left[1 - \left(1 - \frac{C'_2}{\lambda_{\text{eff}}^2} \right)^{1/2} \right] \tag{10–10}$$

where y_{cr} is the deflection corresponding to the onset of instability. Samónov[5] states that this equation is cited by Wahl[6] and verified experimentally by Haringx.[7] The quantity λ_{eff} in Eq. (10–10) is the *effective slenderness ratio* and is given by the equation

$$\lambda_{\text{eff}} = \frac{\alpha L_0}{D} \tag{10–11}$$

C'_1 and C'_2 are elastic constants defined by the equations

$$C'_1 = \frac{E}{2(E - G)}$$

$$C'_2 = \frac{2\pi^2(E - G)}{2G + E}$$

Equation (10–11) contains the *end-condition constant* α. This depends upon how the ends of the spring are supported. Table 10–2 gives values of α for usual end conditions. Note how closely these resemble the end conditions for columns.

Absolute stability occurs when, in Eq. (10–10), the term $C'_2/\lambda_{\text{eff}}^2$ is greater than unity. This means that the condition for absolute stability is that

$$L_0 < \frac{\pi D}{\alpha} \left[\frac{2(E - G)}{2G + E} \right]^{1/2} \tag{10–12}$$

Table 10–2

End-Condition Constants α for Helical Compression Springs*

End Condition	Constant α
Spring supported between flat parallel surfaces (fixed ends)	0.5
One end supported by flat surface perpendicular to spring axis (fixed); other end pivoted (hinged)	0.707
Both ends pivoted (hinged)	1
One end clamped; other end free	2

*Ends supported by flat surfaces must be squared and ground.

[5]Cyril Samónov "Computer-Aided Design," op. cit.

[6]A. M. Wahl, *Mechanical Springs,* 2d ed., McGraw-Hill, New York, 1963.

[7]J. A. Haringx, "On Highly Compressible Helical Springs and Rubber Rods and Their Application for Vibration-Free Mountings," I and II, *Philips Res. Rep.,* vol. 3, December 1948, pp. 401–449, and vol. 4, February 1949, pp. 49–80.

Table 10–4

Constants A and m of $S_{ut} = A/d^m$ for Estimating Minimum Tensile Strength of Common Spring Wires

Source: From *Design Handbook,* 1987, p. 19. Courtesy of Associated Spring.

Material	ASTM No.	Exponent m	Diameter, in	A, kpsi · in^m	Diameter, mm	A, MPa · mm^m	Relative Cost of Wire
Music wire*	A228	0.145	0.004–0.256	201	0.10–6.5	2211	2.6
OQ&T wire†	A229	0.187	0.020–0.500	147	0.5–12.7	1855	1.3
Hard-drawn wire‡	A227	0.190	0.028–0.500	140	0.7–12.7	1783	1.0
Chrome-vanadium wire§	A232	0.168	0.032–0.437	169	0.8–11.1	2005	3.1
Chrome-silicon wire‖	A401	0.108	0.063–0.375	202	1.6–9.5	1974	4.0
302 Stainless wire#	A313	0.146	0.013–0.10	169	0.3–2.5	1867	7.6–11
		0.263	0.10–0.20	128	2.5–5	2065	
		0.478	0.20–0.40	90	5–10	2911	
Phosphor-bronze wire**	B159	0	0.004–0.022	145	0.1–0.6	1000	8.0
		0.028	0.022–0.075	121	0.6–2	913	
		0.064	0.075–0.30	110	2–7.5	932	

*Surface is smooth, free of defects, and has a bright, lustrous finish.

†Has a slight heat-treating scale which must be removed before plating.

‡Surface is smooth and bright with no visible marks.

§Aircraft-quality tempered wire, can also be obtained annealed.

‖Tempered to Rockwell C49, but may be obtained untempered.

#Type 302 stainless steel.

**Temper CA510.

Joerres[8] uses the maximum allowable torsional stress for static application shown in Table 10–6. For specific materials for which you have torsional yield information use this table as a guide. Joerres provides set-removal information in Table 10–6, that $S_{sy} \geq 0.65S_{ut}$ increases strength through cold work, but at the cost of an additional operation by the springmaker. Sometimes the additional operation can be done by the manufacturer during assembly. Some correlations with carbon steel springs show that the tensile yield strength of spring wire in torsion can be estimated from $0.75S_{ut}$. The corresponding estimate of the yield strength in shear based on distortion energy theory is $S_{sy} = 0.577(0.75)S_{ut} = 0.433S_{ut} \doteq 0.45S_{ut}$. Samónov discusses the problem of allowable stress and shows that

$$S_{sy} = \tau_{\text{all}} = 0.56S_{ut} \tag{10–16}$$

for high-tensile spring steels, which is close to the value given by Joerres for hardened alloy steels. He points out that this value of allowable stress is specified by Draft Standard 2089 of the German Federal Republic when Eq. (10–2) is used without stress-correction factor.

[8]Robert E. Joerres, "Springs," Chap. 6 in Joseph E. Shigley, Charles R. Mischke, and Thomas H. Brown, Jr. (eds.), *Standard Handbook of Machine Design,* 3rd ed., McGraw-Hill, New York, 2004.

Table 10–5

Mechanical Properties of Some Spring Wires

Material	Elastic Limit, Percent of S_{ut} Tension	Torsion	Diameter d, in	E Mpsi	E GPa	G Mpsi	G GPa
Music wire A228	65–75	45–60	<0.032	29.5	203.4	12.0	82.7
			0.033–0.063	29.0	200	11.85	81.7
			0.064–0.125	28.5	196.5	11.75	81.0
			>0.125	28.0	193	11.6	80.0
HD spring A227	60–70	45–55	<0.032	28.8	198.6	11.7	80.7
			0.033–0.063	28.7	197.9	11.6	80.0
			0.064–0.125	28.6	197.2	11.5	79.3
			>0.125	28.5	196.5	11.4	78.6
Oil tempered A239	85–90	45–50		28.5	196.5	11.2	77.2
Valve spring A230	85–90	50–60		29.5	203.4	11.2	77.2
Chrome-vanadium A231	88–93	65–75		29.5	203.4	11.2	77.2
A232	88–93			29.5	203.4	11.2	77.2
Chrome-silicon A401	85–93	65–75		29.5	203.4	11.2	77.2
Stainless steel							
A313*	65–75	45–55		28	193	10	69.0
17-7PH	75–80	55–60		29.5	208.4	11	75.8
414	65–70	42–55		29	200	11.2	77.2
420	65–75	45–55		29	200	11.2	77.2
431	72–76	50–55		30	206	11.5	79.3
Phosphor-bronze B159	75–80	45–50		15	103.4	6	41.4
Beryllium-copper B197	70	50		17	117.2	6.5	44.8
	75	50–55		19	131	7.3	50.3
Inconel alloy X-750	65–70	40–45		31	213.7	11.2	77.2

*Also includes 302, 304, and 316.

Note: See Table 10–6 for allowable torsional stress design values.

Table 10–6

Maximum Allowable Torsional Stresses for Helical Compression Springs in Static Applications

Source: Robert E. Joerres, "Springs," Chap. 6 in Joseph E. Shigley, Charles R. Mischke, and Thomas H. Brown, Jr. (eds.), *Standard Handbook of Machine Design,* 3rd ed., McGraw-Hill, New York, 2004.

Material	Maximum Percent of Tensile Strength: Before Set Removed (includes K_W or K_B)	Maximum Percent of Tensile Strength: After Set Removed (includes K_s)
Music wire and cold-drawn carbon steel	45	60–70
Hardened and tempered carbon and low-alloy steel	50	65–75
Austenitic stainless steels	35	55–65
Nonferrous alloys	35	55–65

Figure 10–5

Types of ends used on extension springs. *(Courtesy of Associated Spring.)*

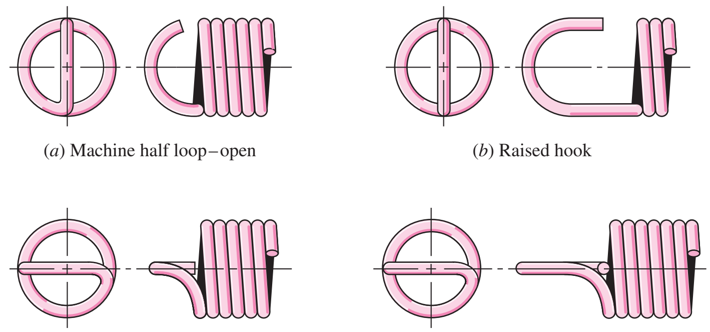

(*a*) Machine half loop–open (*b*) Raised hook

(*c*) Short twisted loop (*d*) Full twisted loop

Figure 10–6

Ends for extension springs. (*a*) Usual design; stress at *A* is due to combined axial force and bending moment. (*b*) Side view of part *a*; stress is mostly torsion at *B*. (*c*) Improved design; stress at *A* is due to combined axial force and bending moment. (*d*) Side view of part *c*; stress at *B* is mostly torsion.

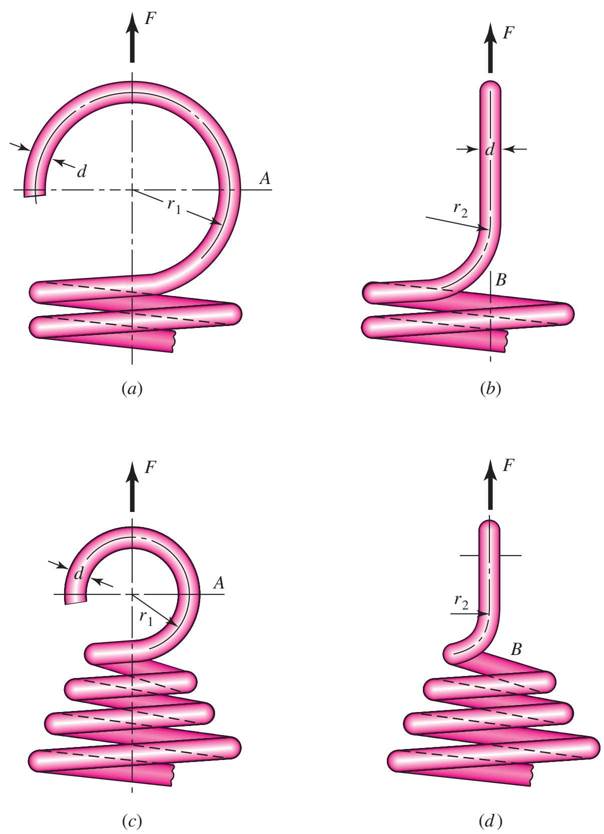

Note: Radius r_1 is in the plane of the end coil for curved beam bending stress. Radius r_2 is at a right angle to the end coil for torsional shear stress.

must be included in the analysis. In Fig. 10–6*a* and *b* a commonly used method of designing the end is shown. The maximum tensile stress at *A*, due to bending and axial loading, is given by

$$\sigma_A = F\left[(K)_A \frac{16D}{\pi d^3} + \frac{4}{\pi d^2}\right] \tag{10–34}$$

where $(K)_A$ is a bending stress-correction factor for curvature, given by

$$(K)_A = \frac{4C_1^2 - C_1 - 1}{4C_1(C_1 - 1)} \qquad C_1 = \frac{2r_1}{d} \tag{10–35}$$

The maximum torsional stress at point B is given by

$$\tau_B = (K)_B \frac{8FD}{\pi d^3} \tag{10–36}$$

where the stress-correction factor for curvature, $(K)_B$, is

$$(K)_B = \frac{4C_2 - 1}{4C_2 - 4} \qquad C_2 = \frac{2r_2}{d} \tag{10–37}$$

Figure 10–6*c* and *d* show an improved design due to a reduced coil diameter.

When extension springs are made with coils in contact with one another, they are said to be *close-wound*. Spring manufacturers prefer some initial tension in close-wound springs in order to hold the free length more accurately. The corresponding load-deflection curve is shown in Fig. 10–7*a*, where y is the extension beyond the free length

Figure 10–7

(*a*) Geometry of the force F and extension y curve of an extension spring; (*b*) geometry of the extension spring; and (*c*) torsional stresses due to initial tension as a function of spring index C in helical extension springs.

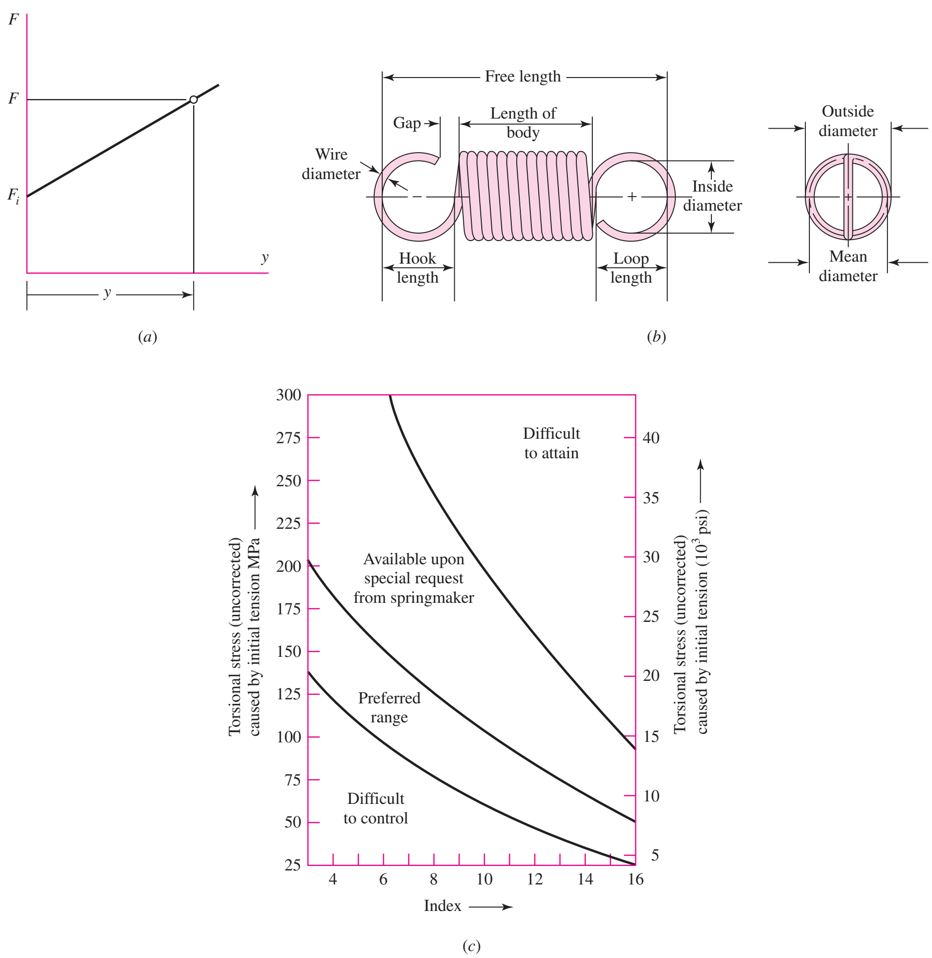

Table 9–3

Minimum Weld-Metal Properties

AWS Electrode Number*	Tensile Strength kpsi (MPa)	Yield Strength, kpsi (MPa)	Percent Elongation
E60xx	62 (427)	50 (345)	17–25
E70xx	70 (482)	57 (393)	22
E80xx	80 (551)	67 (462)	19
E90xx	90 (620)	77 (531)	14–17
E100xx	100 (689)	87 (600)	13–16
E120xx	120 (827)	107 (737)	14

*The American Welding Society (AWS) specification code numbering system for electrodes. This system uses an E prefixed to a four- or five-digit numbering system in which the first two or three digits designate the approximate tensile strength. The last digit includes variables in the welding technique, such as current supply. The next-to-last digit indicates the welding position, as, for example, flat, or vertical, or overhead. The complete set of specifications may be obtained from the AWS upon request.

Table 9–4

Stresses Permitted by the AISC Code for Weld Metal

Type of Loading	Type of Weld	Permissible Stress	n*
Tension	Butt	$0.60S_y$	1.67
Bearing	Butt	$0.90S_y$	1.11
Bending	Butt	0.60–$0.66S_y$	1.52–1.67
Simple compression	Butt	$0.60S_y$	1.67
Shear	Butt or fillet	$0.30S_{ut}^{\dagger}$	

*The factor of safety n has been computed by using the distortion-energy theory.

†Shear stress on base metal should not exceed $0.40S_y$ of base metal.

a welded cold-drawn bar has its cold-drawn properties replaced with the hot-rolled properties in the vicinity of the weld. Finally, remembering that the weld metal is usually the strongest, do check the stresses in the parent metals.

The AISC code, as well as the AWS code, for bridges includes permissible stresses when fatigue loading is present. The designer will have no difficulty in using these codes, but their empirical nature tends to obscure the fact that they have been established by means of the same knowledge of fatigue failure already discussed in Chap. 6. Of course, for structures covered by these codes, the actual stresses *cannot* exceed the permissible stresses; otherwise the designer is legally liable. But in general, codes tend to conceal the actual margin of safety involved.

The fatigue stress-concentration factors listed in Table 9–5 are suggested for use. These factors should be used for the parent metal as well as for the weld metal. Table 9–6 gives steady-load information and minimum fillet sizes.

Table 9–5

Fatigue Stress-Concentration Factors, K_{fs}

Type of Weld	K_{fs}
Reinforced butt weld	1.2
Toe of transverse fillet weld	1.5
End of parallel fillet weld	2.7
T-butt joint with sharp corners	2.0

in which J_u is found by conventional methods for an area having unit width. The transfer formula for J_u must be employed when the welds occur in groups, as in Fig. 9–12. Table 9–1 lists the throat areas and the unit second polar moments of area for the most common fillet welds encountered. The example that follows is typical of the calculations normally made.

Table 9–1

Torsional Properties of Fillet Welds*

Weld	Throat Area	Location of G	Unit Second Polar Moment of Area
1. 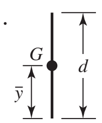	$A = 0.707\,hd$	$\bar{x} = 0$ $\bar{y} = d/2$	$J_u = d^3/12$
2. 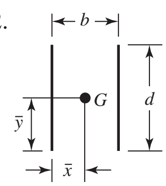	$A = 1.414\,hd$	$\bar{x} = b/2$ $\bar{y} = d/2$	$J_u = \dfrac{d(3b^2 + d^2)}{6}$
3. 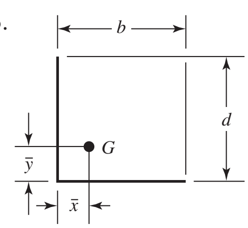	$A = 0.707h(b + d)$	$\bar{x} = \dfrac{b^2}{2(b+d)}$ $\bar{y} = \dfrac{d^2}{2(b+d)}$	$J_u = \dfrac{(b+d)^4 - 6b^2d^2}{12(b+d)}$
4. 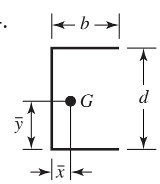	$A = 0.707h(2b + d)$	$\bar{x} = \dfrac{b^2}{2b+d}$ $\bar{y} = d/2$	$J_u = \dfrac{8b^3 + 6bd^2 + d^3}{12} - \dfrac{b^4}{2b+d}$
5. 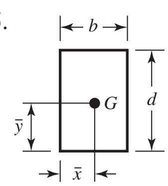	$A = 1.414h(b + d)$	$\bar{x} = b/2$ $\bar{y} = d/2$	$J_u = \dfrac{(b+d)^3}{6}$
6. 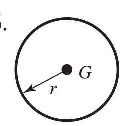	$A = 1.414\,\pi hr$		$J_u = 2\pi r^3$

*G is centroid of weld group; h is weld size; plane of torque couple is in the plane of the paper; all welds are of unit width.

Table 9–2

Bending Properties of Fillet Welds*

Weld	Throat Area	Location of *G*	Unit Second Moment of Area
1. 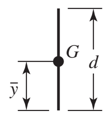	$A = 0.707hd$	$\bar{x} = 0$ $\bar{y} = d/2$	$I_u = \dfrac{d^3}{12}$
2. 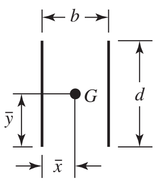	$A = 1.414hd$	$\bar{x} = b/2$ $\bar{y} = d/2$	$I_u = \dfrac{d^3}{6}$
3. 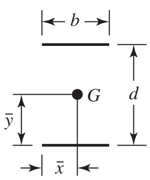	$A = 1.414hb$	$\bar{x} = b/2$ $\bar{y} = d/2$	$I_u = \dfrac{bd^2}{2}$
4. 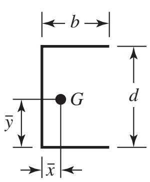	$A = 0.707h(2b + d)$	$\bar{x} = \dfrac{b^2}{2b+d}$ $\bar{y} = d/2$	$I_u = \dfrac{d^2}{12}(6b + d)$
5. 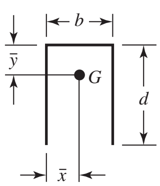	$A = 0.707h(b + 2d)$	$\bar{x} = b/2$ $\bar{y} = \dfrac{d^2}{b+2d}$	$I_u = \dfrac{2d^3}{3} - 2d^2\bar{y} + (b + 2d)\bar{y}^2$
6. 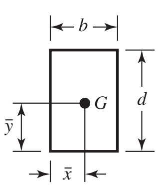	$A = 1.414h(b + d)$	$\bar{x} = b/2$ $\bar{y} = d/2$	$I_u = \dfrac{d^2}{6}(3b + d)$
7. 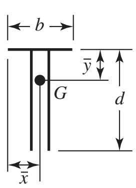	$A = 0.707h(b + 2d)$	$\bar{x} = b/2$ $\bar{y} = \dfrac{d^2}{b+2d}$	$I_u = \dfrac{2d^3}{3} - 2d^2\bar{y} + (b + 2d)\bar{y}^2$

Table 9–2

Continued

Weld	Throat Area	Location of G	Unit Second Moment of Area
8. 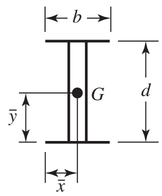	$A = 1.414h(b + d)$	$\bar{x} = b/2$ $\bar{y} = d/2$	$I_u = \frac{d^2}{6}(3b + d)$
9. 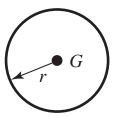	$A = 1.414\pi hr$		$l_u = \pi r^3$

*I_u, unit second moment of area, is taken about a horizontal axis through G, the centroid of the weld group, h is weld size; the plane of the bending couple is normal to the plane of the paper and parallel to the y-axis; all welds are of the same size.

9–5 The Strength of Welded Joints

The matching of the electrode properties with those of the parent metal is usually not so important as speed, operator appeal, and the appearance of the completed joint. The properties of electrodes vary considerably, but Table 9–3 lists the minimum properties for some electrode classes.

It is preferable, in designing welded components, to select a steel that will result in a fast, economical weld even though this may require a sacrifice of other qualities such as machinability. Under the proper conditions, all steels can be welded, but best results will be obtained if steels having a UNS specification between G10140 and G10230 are chosen. All these steels have a tensile strength in the hot-rolled condition in the range of 60 to 70 kpsi.

The designer can choose factors of safety or permissible working stresses with more confidence if he or she is aware of the values of those used by others. One of the best standards to use is the American Institute of Steel Construction (AISC) code for building construction.[4] The permissible stresses are now based on the yield strength of the material instead of the ultimate strength, and the code permits the use of a variety of ASTM structural steels having yield strengths varying from 33 to 50 kpsi. Provided the loading is the same, the code permits the same stress in the weld metal as in the parent metal. For these ASTM steels, $S_y = 0.5S_u$. Table 9–4 lists the formulas specified by the code for calculating these permissible stresses for various loading conditions. The factors of safety implied by this code are easily calculated. For tension, $n = 1/0.60 = 1.67$. For shear, $n = 0.577/0.40 = 1.44$, using the distortion-energy theory as the criterion of failure.

It is important to observe that the electrode material is often the strongest material present. If a bar of AISI 1010 steel is welded to one of 1018 steel, the weld metal is actually a mixture of the electrode material and the 1010 and 1018 steels. Furthermore,

[4]For a copy, either write the AISC, 400 N. Michigan Ave., Chicago, IL 60611, or contact on the Internet at www.aisc.org.

TABLE 12-3
Properties of weld—treating weld as line

Outline of welded joint b = width, d = depth	Bending (about horizontal axis x–x)	Twisting
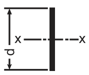	$Z_w = \dfrac{d^2}{6}$	$J_w = \dfrac{d^3}{12}$
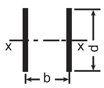	$Z_w = \dfrac{d^2}{3}$	$J_w = \dfrac{d(3b^2 + d^2)}{6}$
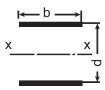	$Z_w = bd$	$J_w = \dfrac{b^3 + 3bd^2}{6}$
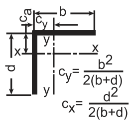	$Z_w = \underset{\text{top}}{\dfrac{4bd + d^2}{6}} = \underset{\text{bottom}}{\dfrac{d^2(4bd + d)}{6(2b + d)}}$	$J_w = \dfrac{(b + d)^4 - 6b^2d^2}{12(b + d)}$
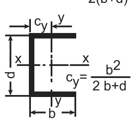	$Z_w = bd + \dfrac{d^2}{6}$	$J_w = \dfrac{(2b + d)^3}{12} - \dfrac{b^2(b + d)^2}{2b + d}$
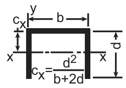	$Z_w = \underset{\text{top}}{\dfrac{2bd + d^2}{3}} = \underset{\text{bottom}}{\dfrac{d^2(2b + d)}{3(b + d)}}$	$J_w = \dfrac{(b + 2d)^3}{12} - \dfrac{d^2(b + d)^2}{b + 2d}$
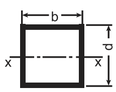	$Z_w = bd + \dfrac{d^2}{3}$	$J_w = \dfrac{(b + d)^3}{6}$
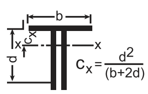	$Z_w = \underset{\text{top}}{\dfrac{2bd + d^2}{3}} = \underset{\text{bottom}}{\dfrac{d^2(2b + d)}{2(b + d)}}$	$J_w = \dfrac{(b + 2d)^3}{12} - \dfrac{d^2(b + d)^2}{b + 2d}$
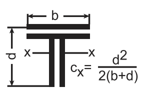	$Z_w = \underset{\text{top}}{\dfrac{4bd + d^3}{3}} = \underset{\text{bottom}}{\dfrac{4bd^2 + d^3}{6b + 3d}}$	$J_w = \dfrac{d^3(4b + d)}{6(b + d)} + \dfrac{b^3}{6}$
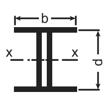	$Z_w = bd + \dfrac{d^2}{3}$	$J_w = \dfrac{b^3 + 3bd^2 + d^3}{6}$
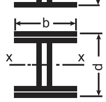	$Z_w = 2bd + \dfrac{d^2}{3}$	$J_w = \dfrac{2b^3 + 6bd^2 + d^3}{6}$
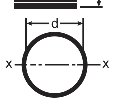	$Z_w = \dfrac{\pi d^2}{4}$	$J_w = \dfrac{\pi d^3}{4}$
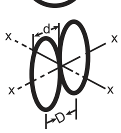	$Z_w = \dfrac{\pi d^2}{2} + \pi D^2$	—
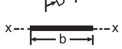	—	$J_w = \dfrac{b^3}{12}$

Note: Multiply the values J_w by the size of the weld w to obtain polar moment of inertia J_o of the weld.

Table 8–1

Diameters and Areas of Coarse-Pitch and Fine-Pitch Metric Threads.*

Nominal Major Diameter d mm	Coarse-Pitch Series: Pitch p mm	Coarse-Pitch Series: Tensile-Stress Area A_t mm^2	Coarse-Pitch Series: Minor-Diameter Area A_r mm^2	Fine-Pitch Series: Pitch p mm	Fine-Pitch Series: Tensile-Stress Area A_t mm^2	Fine-Pitch Series: Minor-Diameter Area A_r mm^2
1.6	0.35	1.27	1.07			
2	0.40	2.07	1.79			
2.5	0.45	3.39	2.98			
3	0.5	5.03	4.47			
3.5	0.6	6.78	6.00			
4	0.7	8.78	7.75			
5	0.8	14.2	12.7			
6	1	20.1	17.9			
8	1.25	36.6	32.8	1	39.2	36.0
10	1.5	58.0	52.3	1.25	61.2	56.3
12	1.75	84.3	76.3	1.25	92.1	86.0
14	2	115	104	1.5	125	116
16	2	157	144	1.5	167	157
20	2.5	245	225	1.5	272	259
24	3	353	324	2	384	365
30	3.5	561	519	2	621	596
36	4	817	759	2	915	884
42	4.5	1120	1050	2	1260	1230
48	5	1470	1380	2	1670	1630
56	5.5	2030	1910	2	2300	2250
64	6	2680	2520	2	3030	2980
72	6	3460	3280	2	3860	3800
80	6	4340	4140	1.5	4850	4800
90	6	5590	5360	2	6100	6020
100	6	6990	6740	2	7560	7470
110				2	9180	9080

*The equations and data used to develop this table have been obtained from ANSI B1.1-1974 and B18.3.1-1978. The minor diameter was found from the equation $d_r = d - 1.226\,869p$, and the pitch diameter from $d_p = d - 0.649\,519p$. The mean of the pitch diameter and the minor diameter was used to compute the tensile-stress area.

Square and Acme threads, whose profiles are shown in Fig. 8–3*a* and *b*, respectively, are used on screws when power is to be transmitted. Table 8–3 lists the preferred pitches for inch-series Acme threads. However, other pitches can be and often are used, since the need for a standard for such threads is not great.

Modifications are frequently made to both Acme and square threads. For instance, the square thread is sometimes modified by cutting the space between the teeth so as to have an included thread angle of 10 to 15°. This is not difficult, since these threads are usually cut with a single-point tool anyhow; the modification retains most of the high efficiency inherent in square threads and makes the cutting simpler. Acme threads

Table 8–3

Preferred Pitches for Acme Threads

d, in	$\frac{1}{4}$	$\frac{5}{16}$	$\frac{3}{8}$	$\frac{1}{2}$	$\frac{5}{8}$	$\frac{3}{4}$	$\frac{7}{8}$	1	$1\frac{1}{4}$	$1\frac{1}{2}$	$1\frac{3}{4}$	2	$2\frac{1}{2}$	3
p, in	$\frac{1}{16}$	$\frac{1}{14}$	$\frac{1}{12}$	$\frac{1}{10}$	$\frac{1}{8}$	$\frac{1}{6}$	$\frac{1}{6}$	$\frac{1}{5}$	$\frac{1}{5}$	$\frac{1}{4}$	$\frac{1}{4}$	$\frac{1}{4}$	$\frac{1}{3}$	$\frac{1}{2}$

are sometimes modified to a stub form by making the teeth shorter. This results in a larger minor diameter and a somewhat stronger screw.

8–2 The Mechanics of Power Screws

A power screw is a device used in machinery to change angular motion into linear motion, and, usually, to transmit power. Familiar applications include the lead screws of lathes, and the screws for vises, presses, and jacks.

An application of power screws to a power-driven jack is shown in Fig. 8–4. You should be able to identify the worm, the worm gear, the screw, and the nut. Is the worm gear supported by one bearing or two?

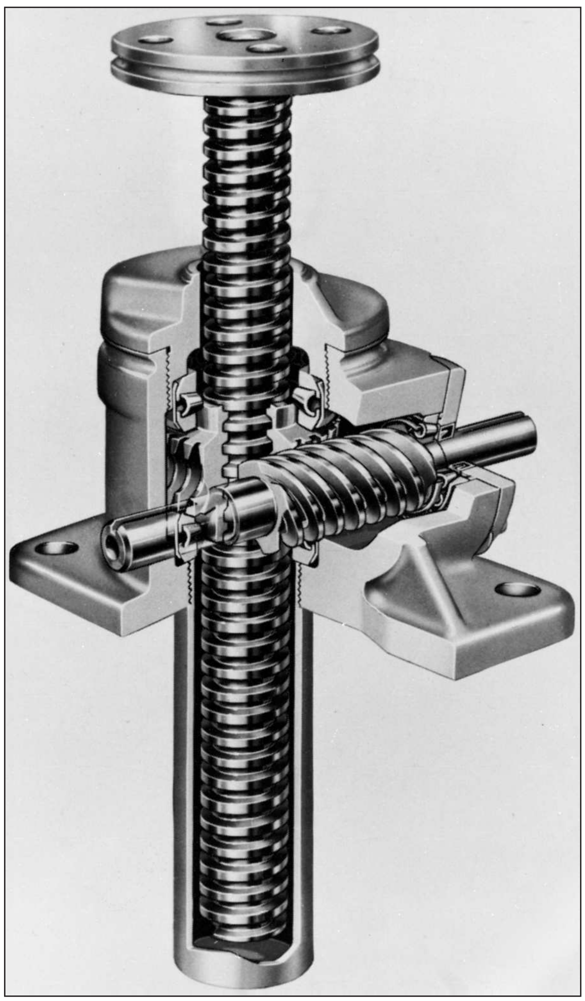

Figure 8–4

The Joyce worm-gear screw jack. *(Courtesy Joyce-Dayton Corp., Dayton, Ohio.)*

Table 8–5

Coefficients of Friction f for Threaded Pairs

Source: H. A. Rothbart and T. H. Brown, Jr., *Mechanical Design Handbook,* 2nd ed., McGraw-Hill, New York, 2006.

Screw Material	Nut Material: Steel	Bronze	Brass	Cast Iron
Steel, dry	0.15–0.25	0.15–0.23	0.15–0.19	0.15–0.25
Steel, machine oil	0.11–0.17	0.10–0.16	0.10–0.15	0.11–0.17
Bronze	0.08–0.12	0.04–0.06	—	0.06–0.09

Table 8–6

Thrust-Collar Friction Coefficients

Source: H. A. Rothbart and T. H. Brown, Jr., *Mechanical Design Handbook,* 2nd ed., McGraw-Hill, New York, 2006.

Combination	Running	Starting
Soft steel on cast iron	0.12	0.17
Hard steel on cast iron	0.09	0.15
Soft steel on bronze	0.08	0.10
Hard steel on bronze	0.06	0.08

common material pairs. Table 8–6 shows coefficients of starting and running friction for common material pairs.

8–3 Threaded Fasteners

As you study the sections on threaded fasteners and their use, be alert to the stochastic and deterministic viewpoints. In most cases the threat is from overproof loading of fasteners, and this is best addressed by statistical methods. The threat from fatigue is lower, and deterministic methods can be adequate.

Figure 8–9 is a drawing of a standard hexagon-head bolt. Points of stress concentration are at the fillet, at the start of the threads (runout), and at the thread-root fillet in the plane of the nut when it is present. See Table A–29 for dimensions. The diameter of the washer face is the same as the width across the flats of the hexagon. The thread length of inch-series bolts, where d is the nominal diameter, is

$$L_T = \begin{cases} 2d + \frac{1}{4}\text{ in} & L \le 6\text{ in} \\ 2d + \frac{1}{2}\text{ in} & L > 6\text{ in} \end{cases} \tag{8–13}$$

and for metric bolts is

$$L_T = \begin{cases} 2d + 6 & L \le 125 \quad d \le 48 \\ 2d + 12 & 125 < L \le 200 \\ 2d + 25 & L > 200 \end{cases} \tag{8–14}$$

where the dimensions are in millimeters. The ideal bolt length is one in which only one or two threads project from the nut after it is tightened. Bolt holes may have burrs or sharp edges after drilling. These could bite into the fillet and increase stress concentration. Therefore, washers must always be used under the bolt head to prevent this. They should be of hardened steel and loaded onto the bolt so that the rounded edge of the stamped hole faces the washer face of the bolt. Sometimes it is necessary to use washers under the nut too.

The purpose of a bolt is to clamp two or more parts together. The clamping load stretches or elongates the bolt; the load is obtained by twisting the nut until the bolt